IEEE Access
Multidisciplinary | Rapid Review | Open Access Journal

Received January 8, 2019, accepted January 16, 2019, date of publication January 24, 2019, date of current version March 7, 2019.

Digital Object Identifier 10.1109/ACCESS.2019.2894658

Single Image-Based Scene Visibility Estimation

QIN LI, YI LI, AND BIN XIE
School of Information Science and Engineering, Central South University, Changsha 410083, China
Corresponding author: Bin Xie (xiebin@csu.edu.cn)

This work was supported by the National Natural Science Foundation of China under Grant 61602520.

ABSTRACT This paper proposes a novel method to utilize a single daylight image of the observed scene to estimate the extinction coefficient of the observed atmosphere and obtain the scene visibility. The proposed method consists of three steps. First, based on the theory of atmospheric physics, we estimate the extinction coefficient of the clear atmosphere in an observed scene. Second, a method combining the dark channel prior and the edge collapse-based transmission refinement is employed to calculate the ratio between the extinction coefficient of the observed atmosphere and that of the clear atmosphere. This ratio indicates the increased degree of the extinction coefficient due to the increment of the atmospheric turbidity. Finally, by multiplying the extinction coefficient of the clear atmosphere and the ratio, the extinction coefficient of the observed atmosphere is calculated and the scene visibility is obtained. The numerous experiments on the proposed method suggest that it performs well in measuring the scene visibility in various types of scenes without additional assistance (e.g., geometric calibration of the camera, road marking extraction, and ground truth data collection).

INDEX TERMS Scene visibility, extinction coefficient, clear atmosphere, image haze removal.

I. INTRODUCTION

Scene visibility is an important issue in meteorological observations. It can not only be used to understand the stability of atmosphere by discriminating the air mass properties, but also reflect the situations of air pollution. Meanwhile, scene visibility estimation is able to assist the development of human society in many aspects. For example, poor scene visibility indicates bad weather which will have a great influence on agricultural production, take-off and landing of aircraft, shipping, and road safety. Therefore, an effective method to estimate scene visibility is of great significance.

Various scene visibility estimation methods have been proposed over the past 20 years. Based on [1], the current scene visibility estimation methods can be classified into four categories.

- **Manual estimation**: Manual estimation means that an observer detects the farthest object by eyes from an observed scene. The distance between the object and the observer is regarded as the scene visibility in the observed scene. This method is drastically influenced by the perception and the reflecting ability of the observer, which will lead to individual bias of scene visibility estimation.
- **Optical sensors**: Commercial products to estimate scene visibility are based on optical sensors, which have been used at airports and weather stations. There are two main optical sensors: transmissometer and forward scattering meter. These sensors only sample in a very limited space, which cannot measure the scene visibility of non-uniform atmosphere. Furthermore, due to the high cost and complex debugging process, optical sensors cannot be densely erected in a large area, which will lead to great difficulty in large-scale scenarios [2], [3].
- **LiDAR**: Based on the analysis of the signal backscattered by fog droplets, scene visibility can be estimated by LiDAR under foggy weather conditions [4]. However, this scene visibility estimation method relies on the fine-tuning of the LiDAR's parameters to adapt itself to the observed atmosphere.
- **Camera-based methods**: With the development of computer vision, the use of camera has attracted more and more interest in scene visibility estimation [5]. There are two kinds of camera-based methods. The first kind is called multi-image based methods for seeking a mapping function between the image information and the scene visibility. Some researchers utilized the image

The associate editor coordinating the review of this manuscript and approving it for publication was Manuel Rosa-Zurera.

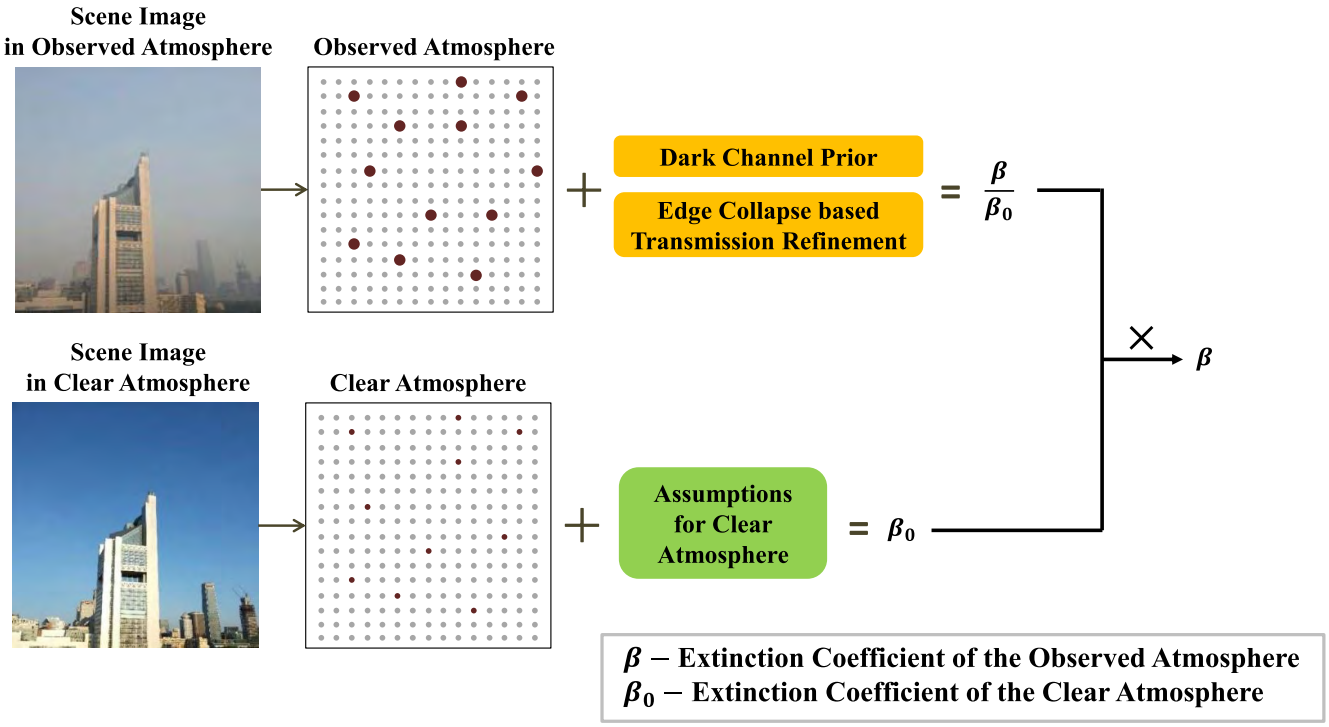

FIGURE 1. Procedure of the proposed method.

contrast to indicate image information, which is always estimated by basic filters such as Sobel, high-pass and homomorphic filters [6], [7]. However, these basic filters are sensitive to illumination variations. To solve this problem, Babari *et al.* [13] used the estimate of the Lambertianess of the image pixels as a weight for the estimated image contrast. Yang [8] proposed an algorithm with the Haar function to improve non-uniform illumination sharpness. In addition, Chaabani *et al.* [1] used a Fourier Transform approach to obtain the global features of scene, which are invariant to illumination changes. Varjo and Hannuksela [34] proposed a kind of image feature vectors which are projections of the High Dynamic Range (HDR) images with lighting normalization. Note that the above methods always need additional reference sensors to collect ground truth data of the scene visibility for a learning phase, which cannot be used for real-time scene visibility estimation. The second kind is called Koschmieder based methods for estimating scene visibility relying on the Koschmieder's law [9]. The Koschmieder's law describes the radiance attenuation through the observed atmosphere from a scene to a sensor and derives a formula to estimate the scene visibility by using the extinction coefficient in the observed scene, which will be introduced later in Section II. Hautière et al. have carried out a series of work along this line [10]–[12], [14], [15]. In such work, the scene visibility is regarded as the distance between the camera and the furthest object. By modeling the geometric calibration of the camera, the parameters of the Koschmieder's law were be calculated and the scene visibility was then obtained. Negru and Nedevschi [16] detected the positions of the inflection point and the horizontal line in an image, and combined the geometric calibration of the camera to estimate the scene visibility. Narasimhan and Nayar [17] developed a physics-based model for the multiple scattering of light rays as when they travel to the sensor, which is able to estimate weather conditions and scene visibility of the observed atmosphere from a single image taken at night. These methods do not need additional reference sensors to collect ground truth data. However, they still require accurate geometric calibration of the camera or scene information, some of which even requires the presence of reference objects with high contrasts.

In order to overcome the drawbacks of current methods, a novel and easy-to-use camera-based method is proposed in this paper. This method belongs to Koschmieder based methods which focuses on calculating the extinction coefficient of the observed atmosphere in an observed scene. Considering that this observed extinction coefficient cannot be obtained by only a single daylight scene image, this paper propose to introduce a prior, i.e., extinction coefficient of the clear atmosphere. This clear extinction coefficient indicates the turbidity of the clear atmosphere, in which 99% of atmospheric particles are air molecules and only 1% are small-scale aerosols. As both air and small-scale aerosols do not affect the turbidity, the clear extinction coefficient should be

very low. Moreover, the constituents of the clear atmosphere in any scene are almost fixed, which means the turbidity of the clear atmosphere remains unchanged. Based on these observations, this paper assumes that the clear extinction coefficient is constant in any observed scene, and deduces this constant relying on the theory of atmospheric physics. Having obtained the clear extinction coefficient, this paper utilizes, a method combining the dark channel prior and the edge collapse based transmission refinement is employed to calculate the ratio between the observed extinction coefficient and the clear extinction coefficient. This ratio indicates the increased degree of the extinction coefficient due to the increment of the atmospheric turbidity. By multiplying the ratio and the clear extinction coefficient, the observed extinction coefficient can be easily obtained. Based on the observed extinction coefficient, the scene visibility is finally estimated based on the Koschmieder's law.

The main contributions of this paper are summarized as follows:

- This paper proposes an assumption: the extinction coefficient of the clear atmosphere is approximately constant in any observed scene. Based on this assumption, this paper deduces a reasonable constant of this clear extinction coefficient relying on theory of atmospheric physics, which is able to simplify the modeling process of air particle and aerosol distributions in the clear atmosphere.
- This paper is the first attempt to put forward a camera-based scene visibility estimation method by using a single daylight image of an observed scene. Although belonging to Koschmieder based methods, the proposed method does not require geometric calibration of the camera. Moreover, experiments have been conducted to validate the accuracy of the proposed method for estimating scene visibility at different levels of atmospheric turbidity.
- The generality of the proposed method has been demonstrated by estimating the scene visibility of daylight scene images in different types of observed scenes.

The rest of this paper is organized as follows. Section II introduces the Koschmieder's law. Section III presents the proposed method in details. Section IV gives the experimental validation. Finally, Section V concludes this paper.

The paper is an extension of our previous work [18] by adding new validation experiments and more detailed analyses.

II. PRELIMINARY KNOWLEDGE

A. THE KOSCHMIEDER'S LAW

The Koschmieder's law [9] describes the daylight imaging process in a scene of the observed atmosphere

$$I = I_0 e^{-\beta d} + I_\infty \left(1 - e^{-\beta d}\right) \tag{1}$$

where I and I_0 are daylight scene images of the observed atmosphere and the clear atmosphere in the same scene, I_∞ is the lightness of the observed atmosphere, β is the extinction coefficient which indicates the atmospheric turbidity of the observed scene. Note that the atmospheric turbidity is homogeneous and then β is identical everywhere in I. d is the distance between the object and the sensor, and $e^{-\beta d}$ is the transmission of the observed atmosphere and indicates the clarity of the observed daylight scene image obtained by the sensor.

On the basis of the Koschmieder's law, Duntley developed a contrast attenuation law [9] — an observed scene with distance d and the intrinsic contrast C_0 will be attenuated by the turbidity of the observed atmosphere, which degrades its contrast to C

$$C = C_0 e^{-\beta d} \tag{2}$$

According to the International Commission of Illumination, the distance d of a black object ($C_0 = 100\%$) with the apparent contrast $C = 5\%$ is regarded as the scene visibility V_{met} (see Eq. (3)).

$$V_{met} = -\log(0.05)/\beta \approx 3/\beta \tag{3}$$

As can be seen, it is essential to calculate the extinction coefficient β before estimating the scene visibility V_{met} in an observed scene, which is the main motivation of this paper.

B. SINGLE IMAGE HAZE REMOVAL METHOD

Research on single image haze removal has attracted increased attention in recent years [36]–[40]. These methods always take advantage of strong prior knowledge or assumptions. For example, Tan [30] assumed that clear images possess higher local contrast than hazy ones. Based on this assumption, images are dehazed by maximized the local contrast. However, images restored via this approach usually tend to be oversaturated. Fattal [35] assumed that the propagation of light projected and the surface shading are partially uncorrelated, and removed haze on the basis of color statistics. Nevertheless, this method does not work for heavily hazed images. He *et al.* [26] proposed the dark channel prior, i.e., most local patches in daylight scene image of the clear atmosphere contain some pixels whose intensity is very low in at least one color channel. They estimated the transmission based on this prior and adopted soft matting for transmission refinement. Although the haze removal performance of [26] is good, it is time-consuming due to the expensive computation of the soft matting. To solve this problem, numerous approaches have been proposed [41]–[46]. He *et al.* [24] replaced the soft matting with the guided filter, which is effective for real-time systems but degrades the visual effects of restored images. Gibson *et al.* [36] presented the median dark channel prior method based on [26], which requires no refinement of the transmission and accelerates the haze removal process. However, the haze removal performance is still unsatisfactory. Chen and Huang [27] proposed an edge collapse-based algorithm by which the transmission can be dynamically repaired and satisfactory haze removal results can be achieved.

III. METHODOLOGY

With the aim to calculate β, we divide the calculation of β into two parts, i.e., calculating β and β respectively. β_0 is the clear extinction coefficient indicating the atmosphere is clear without turbidity. β/β_0 is the ratio between the observed extinction coefficient and the clear extinction coefficient, which indicates the increased degree of the extinction coefficient due to the increment of the atmospheric turbidity. After obtaining β_0 and β/β_0, β can be obtained by

$$\beta = \beta_0 \times \frac{\beta}{\beta_0} \tag{4}$$

Next, we will estimate these two parts, i.e., β_0 and β/β_0.

A. CALCULATION OF β_0

In general, atmosphere is mainly composed of air molecules and aerosol. Air molecules consist of nitrogen, oxygen, noble gas, carbon dioxide, water, and other impurities. Aerosol is a suspension system of liquid or solid particles in the air, of which the large-scale aerosol particles affect the extinction coefficient [19]. In the clear atmosphere, 99% of atmospheric particles are air molecules, and only 1% are small-scale aerosols, both of which have no effect on the extinction coefficient. Moreover, the constituents of the clear atmosphere in any scene are fixed, which means the turbidity of the clear atmosphere remains unchanged. Based on these observations of the clear atmosphere, this paper assumes that the extinction coefficient of the clear atmosphere is approximately constant in any scene.

To deduce this constant, we firstly introduce the formulation of transmittance in the clear atmosphere, which is the degree of solar radiation weakened in vertical direction [20]

$$T_0(\lambda, L) = e^{-\int_0^L \beta_0(\lambda, l)dl} \tag{5}$$

where $\lambda = 0.55\ ^{\mu m}$ and L is the path length of solar radiation. The extinction coefficient of the clear atmosphere β_0 consists of two parts: the clear air molecular extinction coefficient β_{R_0} and the clear aerosol extinction coefficient β_{α_0}

$$\beta_0 = \beta_{R_0} + \beta_{\alpha_0} \tag{6}$$

where β_{R_0} is a known constant [20], i.e., 1.159×10^{-5} (at $\lambda = 0.55\ \mu m$). Based on Eq. (5), the aerosol transmittance of the clear atmosphere is described by

$$T_{\alpha_0}(\lambda, L) = e^{-\int_0^L \beta_{\alpha_0}(\lambda, l)dl} \tag{7}$$

Due to the assumption that the extinction coefficient of the clear atmosphere is approximately constant, Eq.(7) can be simplified:

$$T_{\alpha_0} = e^{-\beta_{\alpha_0} L} = e^{-\beta_{\alpha_0} m_0 H} \tag{8}$$

where H means the effective height of the atmosphere and is always set to $10^4 m$ [21], and m_o is the relative optical mass to describe the relative mass of air on the path of solar radiation [22]. As m_o is unknown, we need to omit m_o in the following steps. Thus, another formulation of aerosol transmittance proposed by *Angstrom* [23] is introduced:

$$T_{\alpha_0} = e^{-\beta_A m_0 \lambda^{-\alpha_w}} \tag{9}$$

where β_A is the Angstrom's turbidity coefficient, and a_w is the wavelength exponent. According to Eq. (8) and Eq. (9), the clear aerosol extinction coefficient β_{α_0} is deduced by

$$\beta_{\alpha_0} = \frac{\beta_A m_0 \lambda^{-a_w}}{L} = \frac{\beta_A m_0 \lambda^{-a_w}}{m_0 H} = \frac{\beta_A \lambda^{-a_w}}{H} \tag{10}$$

Eq. (10) shows that the unknown m_o is successfully omitted. In order to calculate β_{α_0}, the values of β_A and a_w need to be obtained. As suggested in [23], the Angstrom's turbidity coefficient β_A indicates the level of atmospheric turbidity. The cleaner the atmosphere, the smaller the value of β_A. Moreover, the range of β_A is: $0.01 \leq \beta_A \leq 2$ [23]. The wavelength exponent a_w reflects the distribution characteristics of the aerosol particle spectrum. With the increase of the proportion of air molecules in the atmosphere, the value of a_w increases. The range of a_w is: $0.1 \leq a_w \leq 4$ [23]. Considering the extreme situation of the clear atmosphere, i.e., the proportion of air molecules is about 99%, this paper chooses the minimum value of β_A (i.e., 0.01) and the maximum value of a_w (i.e., 4) to calculate β_{α_0} ($\lambda = 0.55\ \mu m$). As a result, the value of β_{α_0} is equal to: $1.093 \times 10^5 m^{-1}$. Based on Eq. (6), β_0 is finally obtained: $2.2518 \times 10^{-5} m^{-1}$.

B. CALCULATION OF β/β_0

For calculating β/β_0 by using a daylight scene image of the observed atmosphere I, this paper introduces the transmission of the observed atmosphere and that of the clear atmosphere in the same observed scene, i.e., $e^{-\beta d}$ and $e^{-\beta_0 d}$. Since the distance d remains invariant with the change of β in an observed scene, β/β_0 can be calculated by

$$\frac{\beta}{\beta_0} = \frac{\ln\left(e^{-\beta d}(x, y)\right)}{\ln\left(e^{-\beta_0 d}(x, y)\right)} \tag{11}$$

Afterward, the core issue of calculating β/β_0 is to compute $e^{-\beta d}(x, y)$ and $e^{-\beta_0 d}(x, y)$ respectively, which can be obtained by the single image removal method. Based on Section II (B), we know that [27] can dynamically refine the transmission and achieve satisfactory haze removal results. Therefore, this paper uses [27], i.e., the edge collapse based method, to refine $e^{-\beta d}(x, y)$ and $e^{-\beta_0 d}(x, y)$ respectively.

We first calculate $e^{-\beta d}(x, y)$ and $e^{-\beta_0 d}(x, y)$ by the dark channel prior. Based on [26], the dark channel prior is expressed by

$$\min_{(i,j)\in\Omega(x,y)} \left(\min_{C\in\{R,G,B\}} \left(I_0^C(i, j) \right) \right) \approx 0 \tag{12}$$

where C is a color channel in RGB color space: $C \in \{R, G, B\}$. $\Omega(x, y)$ is a local patch centered at position (x, y). In order to remove the haze, the dark channel on both sides

of (1) is calculated by

$$\min_{(i,j)\in\Omega(x,y)}\left(\min_{C\in\{R,G,B\}} I\right)=\min_{(i,j)\in\Omega(x,y)}\left(\min_{C\in\{R,G,B\}} I_0\right)e^{-\beta d}+\min_{(i,j)\in\Omega(x,y)}\left(\min_{C\in\{R,G,B\}} I_\infty\right)\left(1-e^{-\beta d}\right) \tag{13}$$

Putting Eq. (12) into Eq. (13), we obtain

$$e^{-\beta d}(x,y)=1-\omega\min_{(i,j)\in\Omega(x,y)}\min_{C\in\{R,G,B\}}\left(\frac{I^C(\Omega(x,y))}{I_\infty^C}\right) \tag{14}$$

where ω is a constant parameter to keep a very small amount of haze for the distant objects and is set to 0.95 according to He *et al.* [26]. I_∞ can be obtained based on [26]. With the $e^{-\beta d}(x,y)$ and I_∞, the daylight scene image of the clear atmosphere $I_0(x,y)$ can be recovered by

$$I_0(x,y)=\frac{I(x,y)-I_\infty}{\max\left(e^{-\beta d}(x,y),t_0\right)}+I_\infty \tag{15}$$

where t_0 is set to restrict $e^{-\beta d}(x,y)$ in case $e^{-\beta d}(x,y)$ is close to zero. Inspired by Eq. (14), $e^{-\beta_0 d}(x,y)$ can be expressed as

$$e^{-\beta_0 d}(x,y)=1-\omega\min_{(i,j)\in\Omega(x,y)}\min_{C\in\{R,G,B\}}\left(\frac{I_0^C(\Omega(x,y))}{I_\infty^C}\right) \tag{16}$$

where.$I_0(x,y)$ is calculated by image haze removal based on Eq. (15).

Having obtained $e^{-\beta d}(x,y)$ and $e^{-\beta_0 d}(x,y)$, we use the edge collapse based method [27] to refine them. The edge attenuation can be represented by using the entropy of gradient magnitude, which can be described as

$$E=-\sum_{x,y\in I}P(G(x,y))\log_2 P(G(x,y)) \tag{17}$$

where E is the entropy of gradient magnitude and $P(G(x,y))$ is the probability mass function of gradient magnitude $G(x,y)$. $G(x,y)$ can be obtained by combining the vertical gradient $G_v(x,y)$ and horizontal gradient $G_h(x,y)$ as follows

$$G(x,y)=\sqrt{G_v^2(x,y)+G_h^2(x,y)} \tag{18}$$

where

$$G_v(x,y)=K_v*I^g(x,y) \tag{19}$$

$$G_h(x,y)=K_h*I^g(x,y) \tag{20}$$

where $*$ is the two-dimensional convolution operation, I^g is the daylight scene image of the observed atmosphere in gray scale. K_v and K_h are the vertical and horizontal Sobel kernels [28]. After calculating the entropy of gradient magnitude E, a self-adjusting parameter γ for different observed scenes can be obtained by

$$\gamma=1+\mathrm{e}^{-\left(\frac{E}{\sigma}\right)^2} \tag{21}$$

where σ is the standard deviation that can be obtained by using a high-boost filter [29]. By using γ, the transmission $e^{-\beta d}(x,y)$ can be refined by

$$e_r^{-\beta d}(x,y)=e_{\max}^{-\beta d}(x,y)\left(\frac{e^{-\beta d}(x,y)}{e_{\max}^{-\beta d}(x,y)}\right)^\gamma \tag{22}$$

where $e_{\max}^{-\beta d}(x,y)$ denotes the maximum intensity of the transmission map $e^{-\beta d}(x,y)$. Similar, $e^{-\beta_0 d}(x,y)$ can be refined by

$$e_r^{-\beta_0 d}(x,y)=e_{\max}^{-\beta_0 d}(x,y)\left(\frac{e^{-\beta_0 d}(x,y)}{e_{\max}^{-\beta_0 d}(x,y)}\right)^\gamma \tag{23}$$

C. CALCULATION OF ROI

As the dark channel prior may not work for some patches in daylight images where the intensities are similar to white color or to the atmospheric light, the refined transmission of these patches is inaccurate. In order to overcome this problem, we attempt to select patches in I where the dark channel prior works, and then calculate $e_r^{-\beta d}$ and $e_r^{-\beta_0 d}$ of these patches for calculating β/β_0. These patches are denoted as ROI. Therefore, how to select ROI is the core issue. According to the dark channel prior, ROI in the daylight scene image of the clear atmosphere I_0 should be the ones where the dark channel values should be the minimum, i.e.

$$\mathrm{ROI}=\arg\min_{(x,y)\in I_0} I^{dark}(\Omega(x,y)) \tag{24}$$

where

$$I^{\mathrm{dark}}(\Omega(x,y))=\min_{(x,y)\in I}\min_{C\in\{R,G,B\}}\left(I^C(\Omega(x,y))\right) \tag{25}$$

Inspired by Eq. (24), we propose an assumption: ROI in daylight scene images of the observed atmosphere should also own the minimum dark channel values. In the following steps, we will prove this assumption.

We first calculate the dark channel of I_0 according to Eq. (25)

$$I_0^{\mathrm{dark}}(\Omega(x,y))=\min_{(x,y)\in I_0}\min_{C\in\{R,G,B\}}\left(I_0^C(\Omega(x,y))\right) \tag{26}$$

As I_0 is degraded to I due to the increase of the atmospheric turbidity, there exists a relationship between $I^{\mathrm{dark}}(\Omega)$ and $I_0^{\mathrm{dark}}(\Omega)$, which can be simply described as

$$I^{\mathrm{dark}}(\Omega(x,y))=I_0^{\mathrm{dark}}(\Omega(x,y))+\Delta I^{\mathrm{dark}}(\Omega(x,y)) \tag{27}$$

where $\Delta I^{\mathrm{dark}}(\Omega)$ indicates the variation of $I^{\mathrm{dark}}(\Omega)$ due to the increment of the atmospheric turbidity. As β indicates the atmospheric turbidity of the observed scene, the change of β (denoted as $\Delta\beta$) determines $\Delta I^{\mathrm{dark}}(\Omega(x,y))$. Moreover, β is identical everywhere in I due to the homogeneity of the observed atmosphere, so is $\Delta\beta$. Based on this, $\Delta I^{\mathrm{dark}}(\Omega(x,y))$ should also be identical everywhere in I, i.e.

$$\Delta I^{\mathrm{dark}}(\Omega(x,y))=\Delta I^{\mathrm{dark}} \tag{28}$$

Based on Eq. (28), Eq. (27) turns to

$$I^{\mathrm{dark}}(\Omega(x,y))=I_0^{\mathrm{dark}}(\Omega(x,y))+\Delta I^{\mathrm{dark}} \tag{29}$$

Algorithm 1 The Procedure of ROI Extraction

Input: An observed daylight scene image I;
Output:ROI
1. Calculate I^{dark} of I;
2. Select $\Omega_{\min}$ with the minimum value $I^{\text{dark}}_{\min}$ of I^{dark};
3. Set a control factor
$\varepsilon : \varepsilon = 20$;
4. Calculate the length L and the width W of I
5. for$i = 1$ to L**do**
6. for$j = 1$ to W**do**
7. Select an pixel (i, j) of I^{dark}
8. if$I^{\text{dark}}_{\min} \le I^{\text{dark}}(i,j) \le I^{\text{dark}}_{\min} + \varepsilon$
9.$I^{\text{dark}}_{\Omega_{\min}}(i,j) = 255$;
10. else
11.$I^{\text{dark}}_{\Omega_{\min}}(i,j) = 0$;
12. end for
13. end for
14. Extract the connected domains in $\Omega_{\min}$;
15. Compute the number of pixels in each connected domain in $\Omega_{\min}$;
16. Extract the connected domain with the maximum number of pixels as ROI.

According to the dark channel prior, the intensity of ROI in I^{dark}_0 is the minimum, i.e.

$$I^{\text{dark}}_0(\Omega) \ge I^{\text{dark}}_0(\text{ROI}) \tag{30}$$

We add ΔI^{dark} to both sides of Eq. (30) and obtain

$$I^{\text{dark}}_0(\Omega) + \Delta I^{\text{dark}} \ge I^{\text{dark}}_0(\text{ROI}) + \Delta I^{\text{dark}} \tag{31}$$

According to Eq. (29), Eq. (31) is equivalent to

$$I^{\text{dark}}(\Omega) \ge I^{\text{dark}}(\text{ROI}) \tag{32}$$

By Eq. (32), we find that I^{dark} in ROI is also the minimum, which validates the assumption, i.e., ROI in I should also own the minimum dark channel values. Based on this assumption, this paper proposes an easy-to-use method to extract ROI automatically. Algorithm I shows the procedure of this method. Steps 1-2 select Ω with the minimum I^{dark} in I(denoted as $\Omega_{\min}$). In order to prevent $\Omega_{\min}$ from being a single pixel, step 3 introduces a factor ε to control the number of pixels in $\Omega_{\min}$. Steps 4-13 select pixels with the value between $I^{\text{dark}}_{\min}$ and $I^{\text{dark}}_{\min} + \varepsilon$. After the above steps, some interference pixels may be wrongly selected. Considering that these interference pixels usually constitute very small connected domains, we propose that the connected domain with the maximum number of pixels should be ROI. Based on this, step 14 extracts the connected domains of $\Omega_{\min}$. Step 15 computes the number of pixels in each connected domain. Step 16 extracts the connected domain with the maximum number of pixels which should finally be ROI.

After obtaining ROI, β/β_0 can be finally obtained by

$$\frac{\beta}{\beta_0} = \frac{\ln\left(e^{-\beta d}(\text{ROI})\right)}{\ln\left(e^{-\beta_0 d}(\text{ROI})\right)} \tag{33}$$

IV. EXPERIMENTAL VALIDATION

A. EFFECTIVENESS OF EDGE COLLAPSE BASED METHOD

In the proposed method, a method combining the dark channel prior and the edge collapse based transmission refinement is introduced for transmission calculation, which greatly affects the performance of β/β_0 calculation as well as the scene visibility estimation. Therefore, it's necessary to validate the effectiveness of this method. To do this, we compared the haze removal performance of this method and other typical haze removal methods which includes Tan [30], He *et al.* [26], Ancuti and Ancuti [31], Zhu *et al.* [32], and Ju *et al.* [33]. We selected three daylight scene images at three levels of haze concentration respectively, i.e., low, medium and high. Fig. 2 shows the results of image haze removal by different methods. Based on the visual inspection, [30] (Fig. 2(b)) results in underestimated color contrast, which cannot obtain a visually pleasing restored image. References [26] (Fig. 2(c)), [31] (Fig. 2(d)), and [32] (Fig. 2(e)) lose some information in the sky areas and have halo effects. Reference [33] (Fig. 2(f)) can achieve good removal results except when the haze concentration is high. When the haze is dense, distant objects of restored images are not well

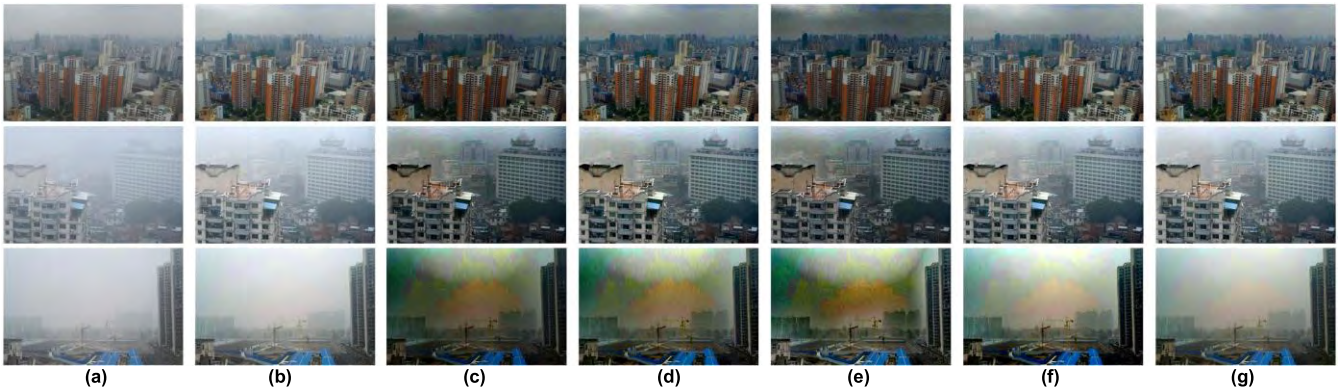

FIGURE 2. Results of image haze removal by different methods. (a) Original image. (b) Tan [30]. (c) He *et al.* [26]. (d) Ancuti and Ancuti [31]. (e) Zhu *et al.* [32]. (f) Ju *et al.* [33]. (g) dark channel prior + edge collapse based transmission refinement.

displayed. In contrast to these methods, the method combining the dark channel prior and the edge collapse based transmission refinement (Fig. 2(g)) can obtain accurate haze removal results and works well at different levels of haze concentration. Compared with [30], the restored images obtained by this method seem more natural. Compared with [26], [31], and [32], this method performs better in preserving the information in the sky areas. Compared with [33], this method performs better when the haze concentration is high, and obtains more accurate information of detail areas in the images with high haze concentration.

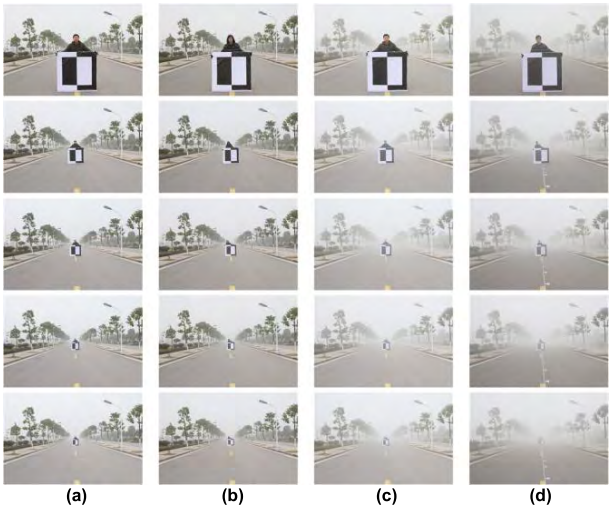

FIGURE 3. Image sequences at four levels of atmospheric turbidity. (a)–(d) Image sequence I to IV.

TABLE 1. Results of β at different positions in four image sequences.

	1	2	3	4	5
I	0.0078	0.0084	0.0077	0.0091	0.0077
II	0.0170	0.0186	0.0187	0.0182	0.0190
III	0.0219	0.0218	0.0216	0.0232	0.0222
IV	0.0260	0.0273	0.0282	0.0278	0.0275

B. RATIONALITY OF β

Due to the homogeneity of the atmosphere, β should be homogeneous in an observed scene. Moreover, with the increase of atmospheric turbidity, the extinction ability of atmospheric particles is enhanced, which makes β increase. To verify the above two characteristics, we made a target board and took five images of the target board at different locations at four levels of atmospheric turbidity. The camera used in our experiment is Canon PowerShot S80. The four image sequences are shown in Fig. 3. We calculated β of each image by the proposed method. TABLE 1 shows the results of β at different locations in four image sequences. Index I to IV indicate four levels of atmospheric turbidity, and the four levels increase in turn. Number 1 to 5 indicate five different positions from near to far. Results show that β rises reasonably with the increase of atmospheric turbidity (see each column in TABLE 1), which satisfies the change rule of β. Meanwhile, values of β at different locations remain almost unchanged at the same level of atmospheric turbidity (see each row in TABLE 1), which proves that β satisfies the homogeneity. Therefore, this experiment offers a powerful validation for the rationality of β calculated by the proposed method.

C. ACCURACY OF THE PROPOSED METHOD

Except for the proposed method, existing Koschmieder based scene visibility estimation methods require accurate geometric calibration of the camera, which makes it impossible for these methods to calculate the scene visibility by using only daylight scene images. As a result, we cannot validate the accuracy by comparing the scene visibility results of the proposed method with those of other Koschmieder based methods. Therefore, we utilized the Columbia Weather and Illumination Database (WILD) [25] to validate the accuracy of the proposed method. WILD owns registered and cali-

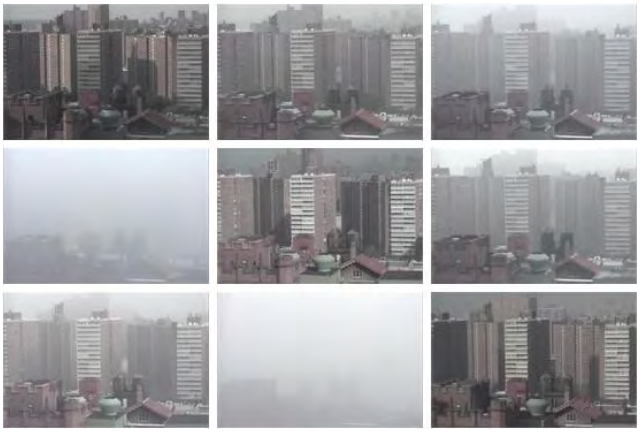

FIGURE 4. Example images of WILD.

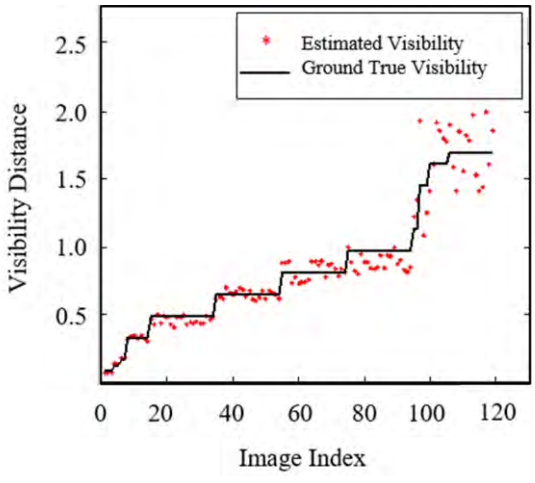

FIGURE 5. The distribution of estimated scene visibility values and ground true visibility values.

TABLE 2. The results of MRE at each level of atmospheric turbidity.

Level of Atmospheric turbidity	I	II	III	IV	V
Scene Visibility Range[m]	0-2000	2000-4000	4000-8000	8000-15000	>15000
Number of Images	8	7	40	45	20
MRE[%]	4.82	8.13	10.79	13.48	18.26

brated images of a fixed outdoor scene captured for over 5 months, which has covered a wide range of illumination conditions, weather conditions and seasons. We selected 120 high-quality daylight scene images along with ground truth scene visibility. Example images of WILD are shown in Fig. 4. β of each image is calculated by the proposed method and the corresponding scene visibility is estimated by Eq. (3). The distribution of estimated scene visibility values are shown in Fig. 5. As can be seen, values of estimated scene visibility follow the trend of ground true scene visibility curve well.

In order to further validate the accuracy of the proposed method at different levels of atmospheric turbidity, we divided the selected daylight scene images into five categories based on their corresponding ground truth visibility values. These five categories representing five levels of atmospheric turbidity are classified based on [20]. Then, we calculated the mean relative error (MRE) between estimated scene visibility V_0 and ground truth scene visibility V_{met}^{ob} at each level of atmospheric turbidity (see Eq. (26)).

$$\mathrm{MRE} = \left(\frac{1}{N} \sum_{i=1}^{N} \frac{V_{met} - V_{met}^{ob}}{V_{met}^{ob}} \right) \times 100\% \tag{34}$$

where N represents the number of daylight scene images at each level of atmospheric turbidity. Table 2 shows the results of MRE at each level of atmospheric turbidity. As it shows, values of MRE at different levels of atmospheric turbidity are all less than 20%, which conforms to the error requirement of scene visibility estimation [20]. This result proves that the proposed method performs well in estimating scene visibility at different levels of atmospheric turbidity.

D. GENERALITY OF THE PROPOSED METHOD IN VARIOUS TYPES OF OBSERVED SCENES

To validate the generality of the proposed method in various types of observed scenes, we selected experimental daylight scene images in three types of scenes: city, road and nature. Fig.5 - Fig.7 show the experimental images in city, road and nature scenes respectively. To further validate the generality of the proposed method, we selected daylight scene images in different levels of atmospheric turbidity in each type of scenes. TABLE 3 - TABLE 5 show the estimated scene visibility V_{met} and the corresponding reference scene visibility V_{met}^{ob}. V_{met}^{ob} is measured by scene visibility meter. In order to highlight the performance of the proposed method, we calculated the relative error (RE) between the estimated

FIGURE 6. Experimental images in city scenes. (a) F6-1. (b) F6-2. (c) F6-3. (d) F6-4.

FIGURE 7. Experimental images in road scenes. (a) F7-1. (b) F7-2. (c) F7-3. (d) F7-4.

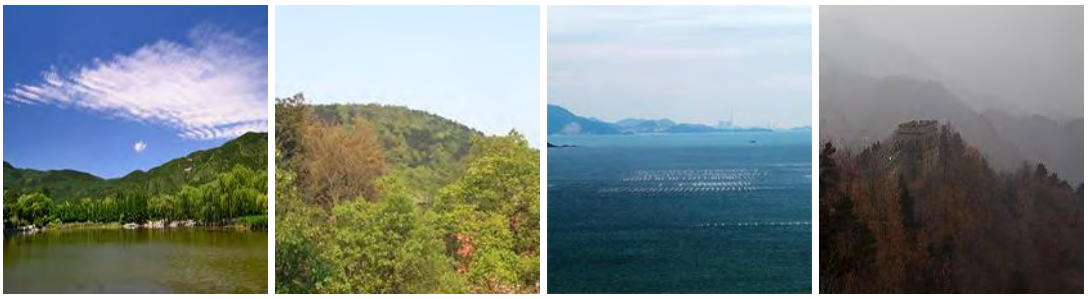

FIGURE 8. Experimental images in nature scenes. (a) F8-1. (b) F8-2. (c) F8-3. (d) F8-4.

TABLE 3. Statistics of V_{met}, V_{met}^{ob}, and RE in city scenes.

Instance	F6-1	F6-2	F6-3	F6-4
V_{met} [m]	19645.00	7174.98	2825.50	915.00
V_{met}^{ob} [m]	24500.00	8100.00	3100.00	1000.00
RE[%]	19.81	11.42	8.87	8.50

TABLE 4. Statistics of V_{met}, V_{met}^{ob}, and RE in city scenes.

Instance	F7-1	F7-2	F7-3	F7-4
V_{met} [m]	20972.61	7192.80	280.36	28.50
V_{met}^{ob} [m]	24500.00	8100.00	300.00	30.00
RE[%]	14.40	11.20	6.55	5.00

TABLE 5. Statistics of V_{met}, V_{met}^{ob}, and RE in city scenes.

Instance	F8-1	F8-2	F8-3	F8-4
V_{met} [m]	19967.76	17205.35	7703.84	5740.80
V_{met}^{ob} [m]	24500.00	15000.00	8900.00	6200.00
RE[%]	18.50	14.70	13.44	5.79

scene visibility V_{met} and the reference V_{met}^{ob} by

$$\mathrm{RE} = \left| \frac{V_{met} - V_{met}^{ob}}{V_{met}^{ob}} \right| \times 100\% \tag{35}$$

where V_{met}^{ob} is measured by a scene visibility meter. TABLE 3–TABLE 5 show the statistics of V_{met}, V_{met}^{ob}, and RE in city, road and nature scenes respectively. These statistical results show that V_{met} is close to V_{met}^{ob} no matter what the observed scene is. And the values of RE are all less than 20%. These results validate that the proposed method works well in various types of observed scenes and has strong generality.

V. CONCLUSION

When measuring the scene visibility of an observed scene, the core issue is to estimate the extinction coefficient β of the observed atmosphere. In this paper, a novel framework for calculating β is proposed. Firstly, this paper assumes that the extinction coefficient of the clear atmosphere β_0 is approximately constant in any scene. Based on this assumption, this paper deduces a reasonable constant of β_0 relying on the theory of atmosphere physics. Then, the ratio β/β_0 is calculated based on a method of combining the Koschmieder' s law and the single image haze removal method. By multiplying β_0 and β/β_0, β is calculated and the scene visibility V_{met} is finally estimated. Without any additional assistance (e.g., geometric calibration of camera, road marking extraction, and ground truth data collection), the proposed method performs well in measuring the scene visibility in various types of scenes by using only a single daylight scene image as input, which might open a new trend in scene visibility estimation.

ACKNOWLEDGMENT

(Qin Li and Yi Li contributed equally to this work.)

REFERENCES

[1] H. Chaabani, F. Kamoun, H. Bargaoui, F. Outay, and A.-Ul-H. Yasar, "A Neural network approach to visibility range estimation under foggy weather conditions," *Procedia Comput. Sci.*, vol. 113, pp. 466–471, Dec. 2017.

[2] S. Park, D.-H. Lee, and Y.-G. Kim, "Development of a transmissometer for meteorological visibility measurement," in *Proc. IEEE Congr. Conf. Lasers Electro-Opt. Pacific Rim (CLEO-PR)*, Aug. 2015, pp. 1–2.

[3] J. Zhang, G. Y. Zhang, G. F. Sun, and J. L. Zhang, "Calibration method for standard scattering plate calibration system used in calibrating scene visibility meter," *Acta Photonica Sinica*, vol. 46, no. 3, pp. 1–9, 2017.

[4] F. Rosenstein, "Intelligent rear light-constant perceptibility of light signals under all weather conditions," in *Proc. Int. Symp. Automot. Lighting (ISAL)*. Prague, Czech Republic: Charles Univ. in Prague, 2005, pp. 403–414.

[5] R. Hallowell, M. Matthews, and P. Pisano, "An automated visibility detection algorithm utilizing camera imagery," in *Proc. 23rd Conf. Interact. Inf. Process. Syst. Meteorol., Oceanogr., Hydrol. (IIPS)*, San Antonio, TX, USA, Jan. 2007, pp. 1–15.

[6] J.-J. Liaw, S.-B. Lian, and R.-C. Chen, "Atmospheric visibility monitoring using digital image analysis techniques," in *Proc. Int. Conf. Comput. Anal. Images Patterns (ICCAIP)*. New York, NY, USA: Springer-Verlag, 2009, pp. 1204–1211.

[7] C.-H. Luo, C.-Y. Wen, C.-S. Yuan, J.-J. Liaw, C.-C. Lo, and S.-H. Chiu, "Investigation of urban atmospheric visibility by high-frequency extraction: Model development and field test," *Atmos. Environ.*, vol. 39, no. 14, pp. 2545–2552, 2005.

[8] C.-C. Yang, "Improving the sharpness of a non-uniformly illuminated image by an integral mask-filtering approach," *Optik*, vol. 124, no. 21, pp. 5049–5051, 2013.

[9] Z. Lee and S. Shang, "Visibility: How applicable is the century-old Koschmieder model?" *J. Atmos. Sci.*, vol. 73, no. 11, pp. 4573–4581, 2016.

[10] N. Hautiére, R. Babari, É. Dumont, R. Brémond, and N. Paparoditis, "Estimating meteorological visibility using cameras: A probabilistic model-driven approach," in *Proc. Asian Conf. Comput. Vis. (ACCV)*. Berlin, Germany: Springer, 2010, pp. 243–254.

[11] R. Gallen, A. Cord, N. Hautière, and D. Aubert, "Towards night fog detection through use of in-vehicle multipurpose cameras," in *Proc. IEEE Intell. Vehicles Symp. (IV)*, Jun. 2011, pp. 399–404.
[12] R. Babari, N. Hautière, E. Dumont, R. Brémond, and N. Paparoditis, "A model-driven approach to estimate atmospheric visibility with ordinary cameras," *Atmos. Environ.*, vol. 45, no. 30, pp. 5316–5324, 2011.
[13] R. Babari, N. Hautière, E. Dumont, J.-P. Papelard, and N. Paparoditis, "Computer vision for the remote sensing of atmospheric visibility," in *Proc. IEEE Int. Conf. Comput. Vis. Workshops (ICCV Workshops)*, Nov. 2011, pp. 219–226.
[14] N. Hautière, J.-P. Tarel, J. Lavenant, and D. Aubert, "Automatic fog detection and estimation of visibility distance through use of an onboard camera," *Mach. Vis. Appl.*, vol. 17, no. 1, pp. 8–20, 2006.
[15] N. Hautière, R. Labayrade, and D. Aubert, "Estimation of the visibility distance by stereovision: A generic approach," *IEICE Trans. Inf. Syst.*, vol. E89-D, no. 7, pp. 2084–2091, 2006.
[16] M. Negru and S. Nedevschi, "Image based fog detection and visibility estimation for driving assistance systems," in *Proc. IEEE 9th Int. Conf. Intell. Comput. Commun. Process. (ICCP)*, Sep. 2013, pp. 163–168.
[17] S. G. Narasimhan and S. K. Nayar, "Shedding light on the weather," in *Proc. IEEE Comput. Soc. Conf. Comput. Vis. Pattern Recognit. (CVPR)*, Jun. 2003, p. 1.
[18] Q. Li and B. Xie, "Visibility estimation using a single image," in *Proc. CCF Chin. Conf. Comput. Vis. (CCCV)*. Singapore: Springer, 2017, pp. 343–355.
[19] C. F. Bohren and D. R. Huffman, *In Absorption and Scattering of Light by Small Particles*. Hoboken, NJ, USA: Wiley, 2014.
[20] K. N. Liou, *An Introduction to Atmospheric Radiation*. New York, NY, USA: Academic, 2002.
[21] A. Berk and F. Hawes, "Validation of MODTRAN 6 and its line-by-line algorithm," *J. Quant. Spectrosc. Radiat. Transf.*, vol. 203, pp. 542–556, Dec. 2017.
[22] B. Sun, R. Ramamoorthi, S. G. Narasimhan, and S. K. Nayar, "A practical analytic single scattering model for real time rendering," *ACM Trans. Graph.*, vol. 24, no. 3, pp. 1040–1049, 2005.
[23] A. Ångström, "The parameters of atmospheric turbidity," *Tellus*, vol. 16, no. 1, pp. 64–75, 1964.
[24] K. He, J. Sun, and X. Tang, "Guided image filtering," *IEEE Trans. Pattern Anal. Mach. Intell.*, vol. 35, no. 6, pp. 1397–1409, Jun. 2013.
[25] S. G. Narasimhan, C. Wang, and S. K. Nayar, "All the images of an outdoor scene," in *Proc. Eur. Conf. Comput. Vis. (ECCV)*. Berlin, Germany: Springer, 2002, pp. 148–162.
[26] K. He, J. Sun, and X. Tang, "Single image haze removal using dark channel prior," *IEEE Trans. Pattern Anal. Mach. Intell.*, vol. 33, no. 12, pp. 2341–2353, Dec. 2011.
[27] B.-H. Chen and S.-C. Huang, "Edge collapse-based dehazing algorithm for visibility restoration in real scenes," *J. Display Technol.*, vol. 12, no. 9, pp. 964–970, Sep. 2016.
[28] S.-C. Huang and S.-Y. Kuo, "Optimization of hybridized error concealment for H.264," *IEEE Trans. Broadcast.*, vol. 54, no. 3, pp. 499–516, Sep. 2008.
[29] M. Gambhir, V. Dhanasekaran, J. Silva-Martinez, and E. Sanchez-Sinencio, "Low-power architecture and circuit techniques for high-boost wide-band G_m-C filters," *IEEE Trans. Circuits Syst. I, Reg. Papers*, vol. 54, no. 3, pp. 458–468, Mar. 2007.
[30] R. T. Tan, "Visibility in bad weather from a single image," in *Proc. IEEE Conf. Comput. Vis. Pattern Recognit.*, Jun. 2008, pp. 1–8.
[31] C. O. Ancuti and C. Ancuti, "Single image dehazing by multi-scale fusion," *IEEE Trans. Image Process.*, vol. 22, no. 8, pp. 3271–3282, Aug. 2013.
[32] Q. Zhu, J. Mai, and L. Shao, "A fast single image haze removal algorithm using color attenuation prior," *IEEE Trans. Image Process.*, vol. 24, no. 11, pp. 3522–3533, Nov. 2015.
[33] M. Ju, D. Zhang, and X. Wang, "Single image dehazing via an improved atmospheric scattering model," *Vis. Comput.*, vol. 33, no. 12, pp. 1613–1625, 2017.
[34] S. Varjo and J. Hannuksela, "Image based visibility estimation during day and night," in *Proc. IEEE Asian Conf. Comput. Vis.*, Nov. 2014, pp. 277–289.
[35] R. Fattal, "Single image dehazing," *ACM Trans. Graph.*, vol. 27, no. 3, 2008, Art. no. 72.
[36] K. B. Gibson, D. T. Vo, and T. Q. Nguyen, "An investigation of dehazing effects on image and video coding," *IEEE Trans. Image Process.*, vol. 21, no. 2, pp. 662–673, Feb. 2012.
[37] B.-H. Chen, S.-C. Huang, C.-Y. Li, and S.-Y. Kuo, "Haze removal using radial basis function networks for visibility restoration applications," *IEEE Trans. Neural Netw. Learn. Syst.*, vol. 29, no. 8, pp. 3828–3838, Aug. 2018.
[38] B. Cai, X. Xu, K. Jia, C. Qing, and D. Tao, "DehazeNet: An end-to-end system for single image haze removal," *IEEE Trans. Image Process.*, vol. 25, no. 11, pp. 5187–5198, Nov. 2016.
[39] D. Eigen, D. Krishnan, and R. Fergus, "Restoring an image taken through a window covered with dirt or rain," in *Proc. IEEE Int. Conf. Comput. Vis.*, Dec. 2013, pp. 633–640.
[40] B.-H. Chen, S.-C. Huang, and F.-C. Cheng, "A high-efficiency and high-speed gain intervention refinement filter for haze removal," *J. Display Technol.*, vol. 12, no. 7, pp. 753–759, Jul. 2016.
[41] S.-C. Huang, B.-H. Chen, and W.-J. Wang, "Visibility restoration of single hazy images captured in real-world weather conditions," *IEEE Trans. Circuits Syst. Video Technol.*, vol. 24, no. 10, pp. 1814–1824, Oct. 2014.
[42] S.-C. Huang, J.-H. Ye, and B.-H. Chen, "An advanced single-image visibility restoration algorithm for real-world hazy scenes," *IEEE Trans. Ind. Electron.*, vol. 62, no. 5, pp. 2962–2972, May 2015.
[43] J.-P. Tarel and N. Hautière, "Fast visibility restoration from a single color or gray level image," in *Proc. IEEE 12th Int. Conf. Comput. Vis.*, Sep./Oct. 2009, pp. 2201–2208.
[44] B.-H. Chen, S.-C. Huang, and J. H. Ye, "Hazy image restoration by bi-histogram modification," *ACM Trans. Intell. Syst. Technol.*, vol. 6, no. 4, 2015, Art. no. 50.
[45] J. Yu and Q. Liao, "Fast single image fog removal using edge-preserving smoothing," in *Proc. IEEE Int. Conf. Acoust., Speech Signal Process.*, May 2011, pp. 1245–1248.
[46] B.-H. Chen and S.-C. Huang, "An advanced visibility restoration algorithm for single hazy images," *ACM Trans. Multimedia Comput., Commun., Appl.*, vol. 11, no. 4, 2015, Art. no. 53.

QIN LI received the B.S. degree in intelligent science and technology and the M.S. degree in automation from Central South University, Changsha, China, in 2015 and 2018, respectively, where she is currently pursuing the Ph.D. degree. Her current research interests include computer vision, pattern recognition, machine learning, and human–robot interaction.

YI LI received the B.S. degree from the College of Information Engineering, Xiang Tan University, Xiangtan, in 2002, and the M.S. and Ph.D. degrees from the School of Information Science and Engineering, Central South University, Changsha, China, in 2005 and 2013, respectively, where he is currently a Lecturer with the Department of Automation Science and Technology. His research interests include computer vision, machine learning, and pattern recognition.

BIN XIE received the B.S. degree in electronic information engineering and the Ph.D. degree in information and communication engineering from Zhejiang University, Hangzhou, China, in 2003 and 2008, respectively. He is currently an Associate Professor with the Department of Automation Science and Technology, Central South University, Changsha, China. His research interests include computer vision, pattern recognition, and robotics.